Journal of Nanomaterials & Molecular Nanotechnology

Research Article

Bundlet Model of Single-Wall Carbon, BC₂N and BN Nanotubes, Cones and Horns in Organic Solvents

Francisco Torrens[1]* and Gloria Castellano[2]

Abstract

The existence of Single-wall C-nanocones (SWNCs), especially nanohorns (SWNHs) and BC_2N/Boron Nitride (BN) analogues is discussed in organic solvents in cluster form. A theory is developed based on the *bundlet* model, describing distribution function by size. The phenomena present unified explanation in the model, in which free energy of (BC_2N/BN-)SWNCs involved in cluster, is combined from two components: volume one proportional to the number of molecules n in cluster and surface one, to $n^{1/2}$. The model enables describing distribution function of (BC_2N/BN-)SWNC clusters by size. From geometrical differences, bundlet [(BC_2N/BN-)SWNCs]/droplet ($C_{60}/B_{15}C_{30}N_{15}/B_{30}N_{30}$) models predict dissimilar behaviours. Various disclination (BC_2N/BN-)SWNCs are studied *via* energetic/structural analyses. Several (BC_2N/BN-)SWNC's ends are studied, which are different because of closing structure and arrangement type. Packing efficiencies and interaction-energy parameters of (BC_2N/BN-)SWNCs/SWNHs are intermediate between $C_{60}/B_{15}C_{30}N_{15}/B_{30}N_{30}$ and (BC_2N/BN-)Single-wall C-nanotube (SWNT) clusters: in-between behaviour is expected; however, properties of (BC_2N/BN-)SWNCs, especially (BC_2N/BN-)SWNHs, are calculated closer to (BC_2N/BN-)SWNTs. Structural asymmetry in different (BC_2N/BN-)SWNCs, characterized by cone angle, distinguishes properties of types: P2. BC_2N/BN, especially species isoelectronic with C-analogues, may be stable.

Keywords

Nanostruture; Solubility of carbon Nanocone; *Bundlet* model for cluster; Droplet model for cluster; Nanohorn; Nanotube; Fullerene; Polymeric boron nitride; Fullerite

Introduction

The interest in nanoparticles arose from the shape-dependent physical properties of nanoscale materials [1,2]. Single-wall C-nanocones (SWNCs) were used to study the nucleation and growth of curved C-structures, suggesting pentagon role. When a pentagonal defect is introduced into a graphitic sheet (graphene) *via* extraction of a 60° sector from the piece, a cone leaf is formed. The presence of pentagons in an SWNC apex is analogue of Single-wall C-nanotube (SWNT) tip topology. Klein group analyzed the eight classes of positive-curvature graphitic nanocones [3-5], and examined the Clar

***Corresponding author:** Francisco Torrens, Institut Universitari de Ciència Molecular, Universitat de València, Edifici d'Instituts de Paterna, P. O. Box 22085, E-46071 València, Spain, Tel: +34 963 544 431; Fax: +34 963 543 274; E mail: francsico.torrens@uv.es*

theory for conjugated C-nanostructures [6-10]. The SWNT ends predicted electronic states related to topological defects in graphite lattice [11]. Resonant picks in the density of states were observed in SWNTs [12], and Multiple-wall C-nanotubes (MWNTs) [13].

The SWNCs with discrete opening angles θ of *ca.* 19°, 39°, 60°, 85° and 113° were observed in C-sample generated by hydrocarbon pyrolysis [14]. Observation was explained by a cone wall model composed of wrapped graphene sheets, where geometrical requirement for seamless connection naturally accounted for semi-discrete character and absolute angles θ. Total disclinations are multiples of 60°, corresponding to number ($P \geq 0$) of pentagons in SWNC apices. Considering graphene-sheet symmetry and the Euler theorem, five SWNC types are obtained from continue graphene sheet, matching to P values in 1–5. Angle θ is given by $\sin(\theta/2)=1–P/6$, leading to flat discs and caped SWNTs, corresponding to $P=0,6$, respectively; the most abundant SWNC with $P=5$ pentagons ($\theta \approx 19°$) is Single-wall C-nanohorn (SWNH). Several configurations exist for given SWNC angle, depending on pentagon arrangement: $\theta \approx 113°$ SWNC contains one pentagon in tip centre and one configuration; other structures show isomers. According to the *Isolated Pentagon Rule* (IPR), those configurations containing isolated pentagons lead to isomers that are more stable than those including grouped ones [15]; another rules were derived form *ab initio* calculations [16]. Covalent functionalization of SWNCs with NH_4^+ improved solubility [17], which was achieved by SWNC skeleton [18-20]/cone-end [21] functionalization and supramolecular π–π stacking interactions [22-24], with pyrenes and porphyrins. An MNDO calculation of BN substitutions in C_{60} showed that analogous one gave $B_{30}N_{30}$ [25]. C-atom substitution in diamond by alternating B/N atoms provided BN-cubic [26]. BN-hexagonal (h) resembles graphite, since it consists of fused planar six-membered B_3N_3 rings; however, interlayer B–N interactions exist. BN nanotubes were visualized [27-29]. BN-h was proposed [30]. BN nanocones were observed [31-33], and calculated [34-39]; the most abundant ones presented 240 and 300° disclinations. BN/AlN nanotube junction was computed [40]. Theoretical studies on BC_2N tubules [41], and graphite-like onion/nanotube production using layered materials, *e.g.* WS_2 [42], MoS_2 [43], BC_2N, BC_3 [44] and BN [45], allowed structures with resistance to oxidation and low thermal/electronic conductivities. The nanostructures of pyrolytically grown $B_xC_yN_z$ were studied: concentration profiles along and across tubes revealed that B, C and N are separated into C/BN domains; compound provides materials that are useful as robust nanocomposites, and semiconductor devices enhanced towards oxidation [46-48]. Dense periodic packings [49,50] of tetrahedra [51], and Platonic solids [52], were examined.

In earlier publications, SWNT [53-58] and (BC_2N/BN-)SWNC [59-61] cluster *bundlet* model was presented. The aim of the present report is to perform a comparative study of different structures, where electrons are globally delocalized. A wide class of phenomena accompanying solution behaviour is analyzed from a unique point of view, taking into account cluster formation. Based on droplet model, (BC_2N/BN-)SWNCs bundlet is examined. The following section describes the computational method. The next section discusses the calculation results. The last section summarizes our conclusions.

Computational Method

Solubility mechanism is based on SWNC cluster formation in solution. Aggregation changes SWNC thermodynamic parameters, which displays phase equilibrium and changes solubility. *Bundlet* model is valid when characteristic SWNC number in cluster $n \gg 1$. In saturated SWNC solution, chemical potentials per SWNC for dissolved substance and crystal, match. Equality is valid for SWNC clusters. Cluster free energy is made up of two parts: volume one proportional to number of SWNCs n in cluster and surface one, to $n^{1/2}$ [62-66]. The model assumes that clusters, consisting of $n \gg 1$ particle, present bundlet shape and permits Gibbs energy G_n for cluster of size n to be:

$$G_n = G_1 n - G_2 n^{1/2} \qquad (1)$$

where $G_{1/2}$ are responsible for contribution to Gibbs energy of molecules, placed inside volume, and on surface of cluster. Chemical potential μ_n of cluster of size n is:

$$\mu_n = G_n + T \ln C_n \qquad (2)$$

where T is absolute temperature. With (1), it results:

$$\mu_n = G_1 n - G_2 n^{1/2} + T \ln C_n \qquad (3)$$

where $G_{1/2}$ are expressed in temperature units. In saturated SWNC solution, cluster-size distribution function is determined *via* equilibrium condition, linking clusters of specified size with solid phase, which corresponds to equality between chemical potentials for SWNCs incorporated into clusters of any size and crystal, resulting in expression for distribution function in saturated solution:

$$f(n) = g_n \exp\left(\frac{-An + Bn^{1/2}}{T}\right) \qquad (4)$$

where A is equilibrium difference between SWNC interaction energies with its surroundings in solid phase, and cluster volume, B, similar difference for SWNCs located on cluster surface and g_n, statistical weight of cluster of size n. One neglects $g_n(n,T)$ dependences in comparison with exponential (4). Normalization for distribution function (4):

$$\sum_{n=1}^{\infty} f(n) n = C \qquad (5)$$

requires $A > 0$, and C is solubility in relative units. As $n \gg 1$, normalization (5) results:

$$C = \overline{g}_n \int_{n=1}^{\infty} n \exp\left(\frac{-An + Bn^{1/2}}{T}\right) dn = \qquad (6)$$

$$C_0 \int_{n=1}^{\infty} n \exp\left(\frac{-An + Bn^{1/2}}{T}\right) dn$$

where $\overline{g}_n$ is statistical weight of cluster averaged over range of n that makes major contribution to integral (6), and C_0, SWNC molar fraction. The A, B and C_0 were taken equal to those for C$_{60}$ in hexane, toluene and CS$_2$: $A=320$ K, $B=970$ K and $C_0=5 \times 10^{-8}$ ($T>260$ K). For polymeric (poly)(BN), A and B were renormalized with regard to B$_{30}$N$_{30}$/C$_{60}$ energies: $A=350$ K and $B=1062$ K. Correction takes into account different packing efficiencies of C$_{60}$/SWNTs/SWNCs:

$$A' = \frac{\eta_{\text{cyl}}}{\eta_{\text{sph}}} A \quad \text{and} \quad B' = \frac{\eta_{\text{cyl}}}{\eta_{\text{sph}}} B \quad \text{(SWNTs)} \quad A' = \frac{\eta_{\text{con}}}{\eta_{\text{sph}}} A \quad \text{and}$$

$$B' = \frac{\eta_{\text{con}}}{\eta_{\text{sph}}} B \quad \text{(SWNCs)} \qquad (7)$$

Where $\eta_{\text{cyl}} = \pi/2(3)^{1/2}$ is cylinder packing efficiency in space (equal to that of circles on plane), $\eta_{\text{sph}} = \pi/3(2)^{1/2}$, that of spheres (Face-centred Cubic, FCC) and η_{con}, that of cones. As $\eta_{\text{sph}} < \eta_{\text{con}} < \eta_{\text{cyl}}$, SWNC behaviour is expected to be intermediate between that of spherical fullerenes and cylindrical SWNTs. Dependences of cluster-size distribution function on concentration and temperature lead to those of thermodynamic and kinetic parameters, characterizing SWNT. For an unsaturated solution, distribution function is determined by clusters equilibrium condition. From Equation (3) one can obtain distribution function *vs.* concentration:

$$f_n(C) = \lambda^n \exp\left(\frac{-An + Bn^{1/2}}{T}\right) \qquad (8)$$

where λ depends on concentration, and is determined by normalization condition:

$$C = C_0 \int_{n=1}^{\infty} n \lambda^n \exp\left(\frac{-An + Bn^{1/2}}{T}\right) dn \qquad (9)$$

where C_0 defines absolute concentration; $C_0 = 10^{-4}$ mol L^{-1} is found by requiring saturation in Equation (9). The formation energy of a cluster of n SWNTs is:

$$E_n = n\left(An - Bn^{1/2}\right) \qquad (10)$$

Using the cluster-size distribution function, one obtains a formula governing the thermal effect of SWNT solution per mole of dissolved substance:

$$H = \frac{\sum_{n=1}^{\infty} E_n f_n(C)}{\sum_{n=1}^{\infty} n f_n(C)} N_a =$$

$$\frac{\sum_{n=1}^{\infty} n\left(An - Bn^{1/2}\right) \lambda^n \exp\left[\left(-An + Bn^{1/2}\right)/T\right]}{\sum_{n=1}^{\infty} n \lambda^n \exp\left[\left(-An + Bn^{1/2}\right)/T\right]} N_a \qquad (11)$$

Where λ depends on the solution total concentration by normalization condition (9). Equations (1)-(11) are modelled in a home-built program available from authors. Droplet cluster model of C$_{60}$ is proposed following modified Equations (1)–(11).

$$G_n = G_1 n - G_2 n^{2/3} \qquad (1)$$

$$\mu_n = G_1 n - G_2 n^{2/3} + T \ln C_n \qquad (3)$$

$$f(n) = g_n \exp\left(\frac{-An + Bn^{2/3}}{T}\right) \qquad (4)$$

$$C = \overline{g}_n \int_{n=1}^{\infty} n \exp\left(\frac{-An + Bn^{2/3}}{T}\right) dn = C_0 \int_{n=1}^{\infty} n \exp\left(\frac{-An + Bn^{2/3}}{T}\right) dn \qquad (6)$$

$$f_n(C) = \lambda^n \exp\left(\frac{-An + Bn^{2/3}}{T}\right) \qquad (8)$$

$$C = C_0 \int_{n=1}^{\infty} n \lambda^n \exp\left(\frac{-An + Bn^{2/3}}{T}\right) dn \qquad (9)$$

$$E_n = n\left(An - Bn^{2/3}\right) \qquad (10)$$

$$H = \frac{\sum_{n=1}^{\infty} E_n f_n(C)}{\sum_{n=1}^{\infty} n f_n(C)} N_a =$$

$$\frac{\sum_{n=1}^{\infty} n\left(An - Bn^{2/3}\right) \lambda^n \exp\left[\left(-An + Bn^{2/3}\right)/T\right]}{\sum_{n=1}^{\infty} n \lambda^n \exp\left[\left(-An + Bn^{2/3}\right)/T\right]} N_a \qquad (11)$$

Calculation Results and Discussion

Table 1 lists the number of pentagons P, disclination angles D_θ, cone apex angles θ, solid angles Ω, number of cones in a sphere, and solid-angle/sphere-covering efficiencies in a graphene hexagonal network. A given disclination, *e.g.* 300° ($P=5$), is usually built by the extraction of one segment generating one distinct cone type (horn). Cone angle decays as the number of pentagons increases from flat discs ($P=0$) to cones ($P=1$-5, *e.g.* SWNHs $P=5$) to tubes ($P=6$). The solid angle results: $\Omega=2\pi\,[1-\cos(\theta/2)]$; the maximum corresponds to the sphere ($P=12$): $\Omega_{sph}=4\pi$. The solid-angle-covering efficiency discards uncomplete SWNCs; sphere-covering efficiency corrects it by packing efficiency of parallel cylinders η_{cyl}: both drop as the number of pentagons increases from discs ($P=0$) to cones ($P=1-5$).

Table 2 collects the packing efficiencies, η, correction factors, and parameters A', B' and C_0, determining molecule interaction energy. As $\eta_{sph} < \eta_{con} < \eta_{cyl}$, cone parameters are intermediate between spheres ($P=12$) and cylinders ($P=6$); *e.g.* the SWNH ($P=5$) parameters are closest to SWNTs ($P=6$).

Table 3 lists the packing parameters: *closeness*, dimension D and efficiency η of equal objects for atom clusters with short-range interaction [67-69].

For closest, not closest, and extremely low packings, packing efficiency, η variations *vs.* packing dimension D (Figure 1), show many superimposed points. On going from $D=$ 2-3, $\eta_{extremely\ low}$ decays quicker than $\eta_{not\ closest/closest}$. For all cases, the packing objects with lower

packing dimension show best fits. The regressions turn out to be:

$$\eta_{closest} = 1.00 + 0.0334D - 0.0400D^2 \qquad (12)$$

$$\eta_{not\ closest} = 1.00 + 0.0125D - 0.0463D^2, \; n=16\ r=0.833,\ s=0.093, \; F=14.8 \qquad (13)$$

Where n is the number of points, r, correlation coefficient, s, standard deviation, and F, Fischer ratio. Results are improved if data for tetrahedra I-IV and truncated tetrahedron I are suppressed:

$$\eta_{not\ closest} = 1.00 + 0.0192D - 0.0497D^2, \; n=11\ r=0.942,\ s=0.054, \; F=31.3 \qquad (14)$$

For extremely low packing:

$$\eta_{extremely\ low} = 1.00 - 0.317D \qquad (15)$$

The parabolic nature of Equations (12)-(14) suggests that linearization would be achieved, if the reciprocal packing dimension D^{-1} is used as abscissa instead of D. For closest, not closest, and extremely low packings, the packing efficiency η variations *vs.* D^{-1} (Figure 2) show many superimposed points. The $\eta_{extremely\ low}$ raises quicker than $\eta_{not\ closest}$, than $\eta_{closest}$.

Again the packing objects with lower packing dimension D present best fits, which result:

$$\eta_{closest} = 0.408 + 0.999D^{-1} \qquad (16)$$

$$\eta_{not\ closest} = 0.182 + 1.31D^{-1} \qquad (17)$$

$n=15\ r=0.780,\ S=0.093,\ F=20.2\ \text{MAPE}=9.10\%\ \text{AEV}=0.3916$

Table 1: Numbers of pentagons (P) and cones, angles and covering efficiencies in graphene hexagonal network.

P[a]	Disclination angle [°]	Cone angle [°]	Solid angle [sr]	No. of cones	Solid-angle-covering efficiency	Sphere-covering efficiency
0	0	180.00	6.28319	2	1.00000	0.90690
1	60	112.89	2.81002	4	0.89446	0.81118
2	120	83.62	1.59998	7	0.89125	0.80828
3	180	60.00	0.84179	14	0.93782	0.85051
4	240	38.94	0.35934	34	0.97225	0.88173
5	300	19.19	0.08788	142	0.99306	0.90060
6	360	0.00	0.00000	∞	1.00000	0.90690
12	720	360.00	12.56637	1	1.00000	0.90690

[a]$P=0$ (disc), 1–5 (cone), 5 (horn), 6 (tube), 12 (sphere).

Table 2: Packing-efficiencies and parameters determining molecule interaction energy; C_0=5×10⁻⁸ (molar fraction).

Molecule	No. of pentagons[a]	Packing efficiency	η-correction factor	A' [K]	B' [K]
SWNC η-correction[b]	0	0.90690	1.22474	392	1188
	1	0.81118	1.09548	351	1063
	2	0.80828	1.09156	349	1059
	3	0.85051	1.14859	368	1114
	4	0.88173	1.19075	381	1155
	5	0.90060	1.21624	389	1180
SWNT η-correction[c]	6	0.90690	1.22474	392	1188
C_{60}-face-centred cubic[d]	12	0.74048	1.00000	320	970

[a] $P=0$ (disc), 1–5 (cone), 5 (horn), 6 (tube), 12 (sphere).
[b] SWNC: Single-wall Carbon Nanocone.
[c] SWNT: Single-wall Carbon Nanotube.
[d] For $T>260$ K.

Table 3: Objects, closeness, packing dimensions *D* and efficiencies *η* for equal objects.

Objects	Closeness	D	Packing efficiency
Low-density Sphere (LDS) I	Extremely low	3	0.042
Low-density Sphere (LDS) II	Extremely low	3	0.045
Low-density Sphere (LDS) III	Extremely low	3	0.056
Tetrahedron I	Not closest	3	18/49=0.36735
Sphere Simple Cubic (SC)	Not closest	3	$\frac{\pi}{6} \approx 0.52360$
Sphere Random *Loose* (RL)	Not closest	3	0.601 ± 0.005
Sphere Random Close (RC)	Not closest	3	0.6366 ± 0.0005
Tetrahedron II	Not closest	3	2/3 = 0.66667
Sphere body-centred cubic (BCC)	Not closest	3	$\frac{\pi\sqrt{3}}{8} \approx 0.68017$
Truncated tetrahedron I	Not closest	3	207/304=0.68092
Tetrahedron III	Not closest	3	17/24=0.70833
Tetrahedron IV	Not closest	3	$\frac{139 + 40\sqrt{10}}{369} \approx 0.71949$
Sphere (FCC alias cubic closest packing, CCP or hexagonal closest packing, HCP)	Closest	3	$\frac{\pi}{3\sqrt{2}} \approx 0.74048$
Tetrahedron V	–	3	0.7786
Tetrahedron VI	–	3	0.7820
Truncated icosahedron	–	3	0.78499
Snub cube	–	3	0.78770
Snub dodecahedron	–	3	0.78864
Rhombic icosidodecahedron	–	3	0.80471
Tetrahedron VII	–	3	0.8226
Truncated icosidodecahedron	–	3	0.82721
Icosahedron	–	3	0.83636
Truncated cubeoctahedron	–	3	$\frac{99}{992}\sqrt{66} - \frac{231}{1984}\sqrt{33} + \frac{2835}{992}\sqrt{2} - \frac{6615}{1984} = 0.84937$
Tetrahedron VIII	–	3	0.85027
Tetrahedron IX	–	3	100/117=0.85470
Tetrahedron X	–	3	4000/4671=0.85635
Icosidodecahedron	–	3	0.86472
Rhombic cubeoctahedron	–	3	$\frac{16\sqrt{2} - 20}{3} = 0.87581$
Truncated dodecahedron	–	3	0.89779
Dodecahedron	–	3	0.90451
Cubeoctahedron	–	3	45/49=0.91837
Octahedron	–	3	18/19=0.94737
Truncated tetrahedron II	–	3	23/24=0.95833
Truncated cube	–	3	$\frac{9}{5 + 3\sqrt{2}} = 0.97375$
Truncated tetrahedron III	–	3	207/208=0.99519
Cube	Closest	3	1.0
Truncated octahedron	Closest	3	1.0
Cylinder in space as square packing (SP) of circles on a plane	Not closest	2	$\frac{\pi}{4} \approx 0.78540$
Cone (*P*=2)	Not closest	2	0.80828
Cone (*P*=1)	Not closest	2	0.81118
Cone (*P*=3)	Not closest	2	0.85051
Cone (*P*=4)	Not closest	2	0.88173
Cone (*P*=5, horn)	Not closest	2	0.90060
Cylinder (as hexagonal packing of circles on a plane)	Closest	2	$\frac{\pi}{2\sqrt{3}} \approx 0.90690$

where Mean Absolute Percentage Error (MAPE) is 9.10% and Approximation Error Variance (AEV), 0.3916. Results are improved if data for tetrahedra I-IV and truncated tetrahedron I are suppressed:

$$\eta_{\text{not closest}} = 0.152 + 1.38 D^{-1} \qquad (18)$$

$n = 10$ $r = 0.918$, $S = 0.054$, $F = 42.9$ MAPE=6.38% AEV=0.2366

And AEV decays by 40%. For extremely low packing:

$$\eta_{\text{extremely low}} = -0.589 + 1.91 D^{-1} \qquad (19)$$

The rising rate of packing efficiency η vs. D^{-1} increases from closest to not closest to extremely low packing efficiencies. Linear Equations (15)–(19) perform better for extrapolations than quadratic Equations (12)–(14). Property-*closeness* inclusion allows performing joint linear fit for $\eta_{\text{closest}}/\eta_{\text{not closest}}$:

$$\eta = 0.180 + 0.0976\,\text{closeness} + 1.31 D^{-1}$$

$n = 12$ $r = 0.924$, $S = 0.053$, $F = 26.5$ MAPE=5.17% AEV=0.1453 (20)

and AEV drops by 63%. One more time, the packing objects with lower packing dimension show the best fit. The quadratic-term inclusion allows the best model:

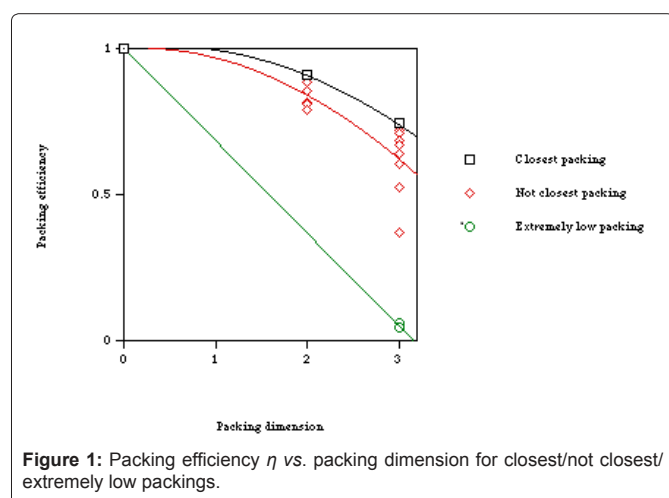$$\eta = 1.00 + 0.0102 D + 0.0381\,\text{closeness} \cdot D - 0.0455 D^2, \quad n = 18$$

Figure 1: Packing efficiency η vs. packing dimension for closest/not closest/ extremely low packings.

Figure 2: Packing efficiency vs. reciprocal dimension for closest/not closest/ extremely low packings.

$r = 0.847$, $S = 0.089$, $F = 11.9$ \hfill (21)

Results are improved if the data for tetrahedra I-IV and truncated tetrahedron I are suppressed:

$$\eta = 1.00 + 0.0151 D + 0.0402\,\text{closeness} \cdot D - 0.0481 D^2$$

$n = 13$ $r = 0.946$, $S = 0.051$, $F = 25.6$ MAPE=4.34% AEV=0.1050 (22)

And AEV decreases by 73%. Once more the packing objects with lower packing dimension present the best fit. Quadratic Equations (21)/(22) perform better than linear equation (17) for intrapolation. Predictions for packing objects with lower packing dimension show an improvement; *e.g.*, for sphere (C_{60})/cylinder (SWNT), the results are quite good.

Table 4 reports the disclination angles D_{θ}, numbers of 2-membered rings (2MR), squares S and pentagons P, and cone apex angles θ in a poly(BN) hexagonal network. A given disclination, *e.g.* 240°, can be built by extraction of one segment generating one distinct cone type (2MR=S=P=0); however, the same disclination can be derived by extraction of two separated segments of 120° each (S=1, P=2), or four unconnected segments of 60° each (S=0, P=4). The cone angles decay as numbers of 2MR, squares or pentagons increase from flat discs (D_{θ}=0°, 2MR=S=P=0) to cones (D_{θ}=60-300°, 2MR=0–1, S=0–2, P=0–5) to tubes (D_{θ}=360°, 2MR=0, S=0–3, P=0–6). The structures observed in BN cones are attributed to lower energy of squares, compared with pentagons; indeed, B–N present higher stability than B–B than N–N bonds, e.g., the line defect D_{θ}=300° and 2MR=S=P=0 would consist of B–B bonds.

The equilibrium difference between Gibbs free energies of interaction of an SWNC with its surroundings, in solid phase and cluster volume/on surface (Figure 3), shows that results for $B_{15}C_{30}N_{15}/B_{30}N_{30}$ are superimposed on C_{60}, and (BC_2N/BN-)SWNC/SWNT on SWNT. On going from C_{60} (droplet) to SWNT (*bundlet*), minimum is less marked (68% of C_{60}), which causes lesser number of units in (BC_2N/BN-)SWNT/SWNCs ($n_{\text{min}} \approx 2$), than in $C_{60}/B_{15}C_{30}N_{15}/B_{30}N_{30}$ clusters (≈8). Moreover, abscissa is longer in $C_{60}/B_{15}C_{30}N_{15}/B_{30}N_{30}$ ($n_{\text{abs}} \approx 28$), than in ($BC_2N/BN$-)SWNT/SWNCs (≈9). When going from C_{60} to $B_{15}C_{30}N_{15}$ to $B_{30}N_{30}$ (or from SWNT to BC_2N- to BN-SWNT, or from SWNCs to BC_2N- to BN-SWNCs), the minimum is increasingly emphasized (4.6% and 9.5%, respectively), while it contains the same number of units. In the SWNCs/BC_2N-SWNCs/ BN-SWNCs (bundlet), the minima result 61–67% of $C_{60}/B_{15}C_{30}N_{15}/B_{30}N_{30}$, similar to those in ($BC_2N/BN$-)SWNT.

The temperature dependence of SWNC solubility, figure 4 shows that results for (BC_2N/BN-)SWNC/SWNT are superimposed on SWNT. Solubility decays with temperature because of cluster formation. At $T \approx 260$ K, C_{60}-crystal presents an orientation disorder phase transition from FCC to Simple Cubic (SC). The solubility decays are less marked for (BC_2N/BN-)SWNT/SWNCs, in agreement with lesser numbers of units in clusters (Figure 3). In particular, at T=260 K, on going from C_{60} to $B_{15}C_{30}N_{15}$ to $B_{30}N_{30}$ (droplet), solubility rises by 22.8% and 52.5%, respectively. When going from C_{60} (droplet) to SWNT (bundlet), solubility decays to 2.6% of C_{60}; SWNCs (bundlet) solubility drops to 2.0–2.5% of C_{60}. On going from $B_{15}C_{30}N_{15}$ (droplet) to BC_2N-SWNT (bundlet), solubility decreases to 2.4% of $B_{15}C_{30}N_{15}$; from $B_{30}N_{30}$ to BN-SWNT (bundlet), solubility diminishes to 2.2% of $B_{30}N_{30}$; BC_2N/BN-SWNCs solubilities decay to 1.8-2.3% of $B_{15}C_{30}N_{15}$ and 1.6–2.1% of $B_{30}N_{30}$.

The cluster distribution function by size in SWNC solution in
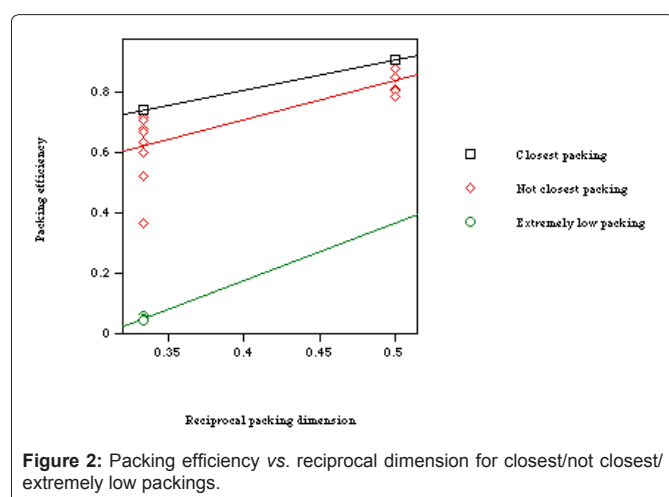
**Table 4:** Angles, numbers of 2-membered rings (2MR), squares *S* and pentagons *P* in a poly(BN) hexagonal network.

Disclination angle [º]	2MR	S	P	Cone angle [º]
0	0	0	0	180.00
60	0	0	1	112.89
120	0	1	0	83.62
120	0	0	2 in opposed ends of an edge	83.62
120	0	0	2 neighbours	83.62
120	0	0	2 isolated by a hexagon	83.62
180	0	0	3 in line	60.00
180	0	0	3 in an arrangement such that each ring has 2 pentagons as nearest neighbours	60.00
180	0	0	3 isolated by a hexagon	60.00
180	0	1	1	60.00
240	0	0	0; 2 2-co-ordinated atoms at the apex	38.94
240	0	0	4 isolated by 2 hexagons	38.94
240	0	0	4 neighbours sharing 2 3-co-ordinated atoms at the apex	38.94
240	0	1	2	38.94
240	0	2	0	38.94
240	1	0	0	38.94
300	0	0	0; line defect consisting of like bonds	19.19
300	0	0	5	19.19
360	0	0	6	0.00
360	0	3	0	0.00
720	0	0	12	360.00

CS$_2$, calculated for saturation concentration at solvent temperature *T*=298.15 K (Figure 5), shows that the results for B$_{15}$C$_{30}$N$_{15}$/B$_{30}$N$_{30}$ are superimposed on C$_{60}$, and (BC$_2$N/BN-)SWNC/SWNT on SWNT. On going from C$_{60}$/B$_{15}$C$_{30}$N$_{15}$/B$_{30}$N$_{30}$ (droplet) to (BC$_2$N/BN-)SWNT/SWNCs (bundlet), the maximum cluster size decays from $n_{max} \approx 8$ to ≈ 2, and distribution is narrowed in agreement with lesser number of units in clusters (Figure 3).

The concentration dependence of the heat of solution in toluene, benzene and CS$_2$, calculated at solvent temperature *T*=298.15 K
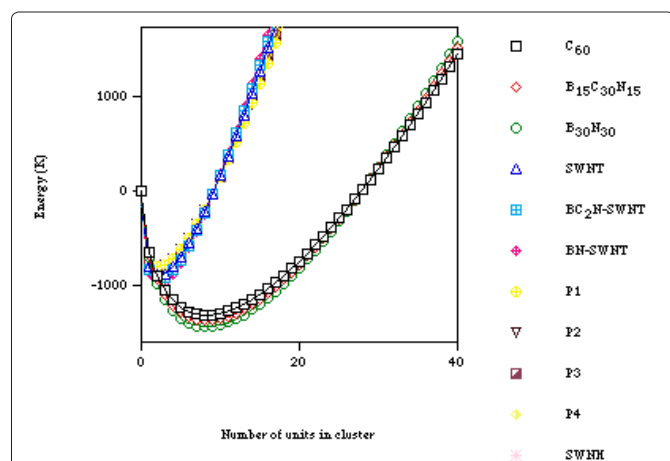
Figure 3: C$_{60}$/B$_{15}$C$_{30}$N$_{15}$/B$_{30}$N$_{30}$–(BC$_2$N/BN-)SWNT–SWNH interaction energy with surroundings in cluster volume/surface.
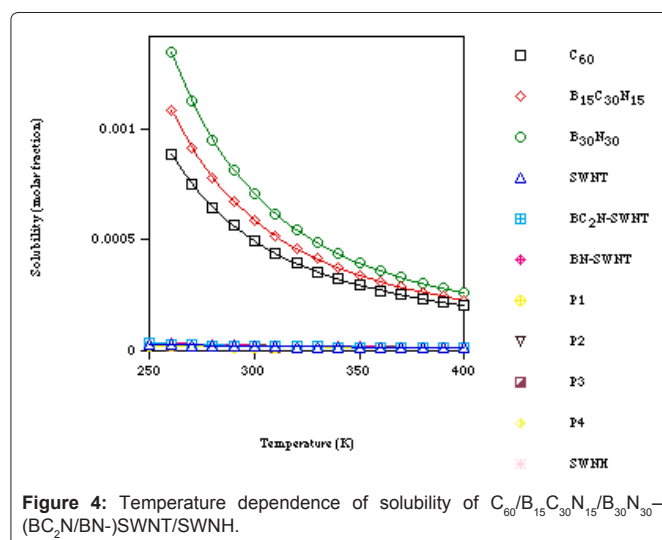
Figure 4: Temperature dependence of solubility of C$_{60}$/B$_{15}$C$_{30}$N$_{15}$/B$_{30}$N$_{30}$– (BC$_2$N/BN-)SWNT/SWNH.

(Figure 6), shows that the results for SWNH are superimposed on SWNT, BC$_2$N-SWNH on BC$_2$N-SWNT, and BN–SWNH on BN–SWNT. For C$_{60}$ (droplet), on going from *C*<0.1% of saturated (<*n*>≈1) to *C*=15% (<*n*>≈7), the heat of solution decays by 73%. In turn for SWNT (bundlet), the heat of solution increases by 54% in the same range, in agreement with lesser number of units in clusters (Figures 3 and 5). In SWNCs (bundlet), the heat of solution augments by 55–80%, in accordance with smaller aggregations. In B$_{15}$C$_{30}$N$_{15}$ (droplet), the heat of solution drops by 74%; in turn for BC$_2$N-SWNT

(bundlet), the heat of solution rises by 49% in agreement with smaller clusters. In BC₂N-SWNCs (bundlet), the heat of solution enlarges by 50-63%, in accordance with smaller aggregations. In $B_{30}N_{30}$ (droplet), the heat of solution decays by 73%; in turn for BN-SWNT (bundlet), the heat of solution increases by 44% in agreement with smaller clusters. In BN-SWNCs (bundlet), the heat of solution enlarges by 45–57%, in accordance with smaller aggregations. The discrepancy between the various experimental data of the heat of solution of fullerenes, poly(BC₂N/BN) and (BC₂N/BN-)SWNT/ SWNCs may be ascribed to the sharp concentration dependence of the heat of solution. The effect of different number of pentagons *P* on concentration dependence shows that the results for SWNC P2 are superimposed on P1, and SWNH on SWNT. The heat of solution varies: P2≈ P1>P3>P4>SWNH≈SWNT >> C₆₀.

Figure 7 displays the temperature dependence of the heat of solution in toluene, benzene and CS₂ calculated for the saturation concentration. The results for SWNH are superimposed on SWNT, BC₂N-SWNH on BC₂N-SWNT, and BN-SWNH on BN-SWNT. The data of C₆₀, etc. are plotted for *T*>260 K after FCC/SC transition. For C₆₀ (droplet) on going from *T*=260 K to *T*=400 K, the heat of solution increases 2.7 kJ mol⁻¹. For SWNT and SWNCs (bundlet), the heat of solution augments 10.4 and 10.4–10.9 kJmol⁻¹, respectively, in the same range. For $B_{15}C_{30}N_{15}$ (droplet), the heat of solution rises to 2.5 kJmol⁻¹. For BC₂N-SWNT and BC₂N-SWNCs (bundlet), the heat of solution augments 10.2 and 10.2–10.7 kJmol⁻¹. For $B_{30}N_{30}$ (droplet), the heat of solution enlarges 2.3 kJmol⁻¹. For BN-SWNT and BN-SWNCs (bundlet), the heat of solution rises 9.9 and 10.0–10.5 kJmol⁻¹.

The results for the dependence of diffusion coefficient on concentration in toluene, at *T*=298.15 K (Figure 8), show that the data for SWNH are superimposed on SWNT, BC₂N-SWNH on BC₂N-SWNT, and BN-SWNH on BN-SWNT. The cluster formation in a solution close to saturation decreases diffusion coefficients by 56%, 69% and 69–71% for C₆₀, SWNT and SWNCs, respectively, as compared with that for C₆₀ molecule. For SWNT (bundlet) diffusion coefficient drops by 29% and for SWNCs (bundlet) diffusion coefficients, by 29–33%, with regard to C₆₀ (droplet). Cluster formation close to saturation diminishes diffusion coefficients by 56%, 68% and
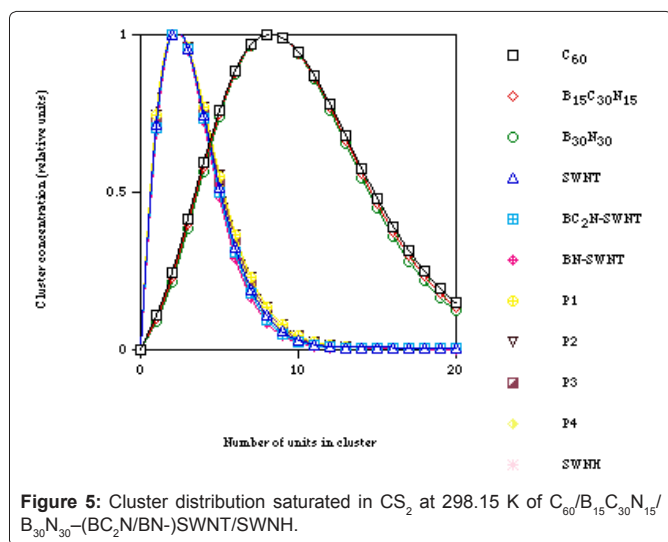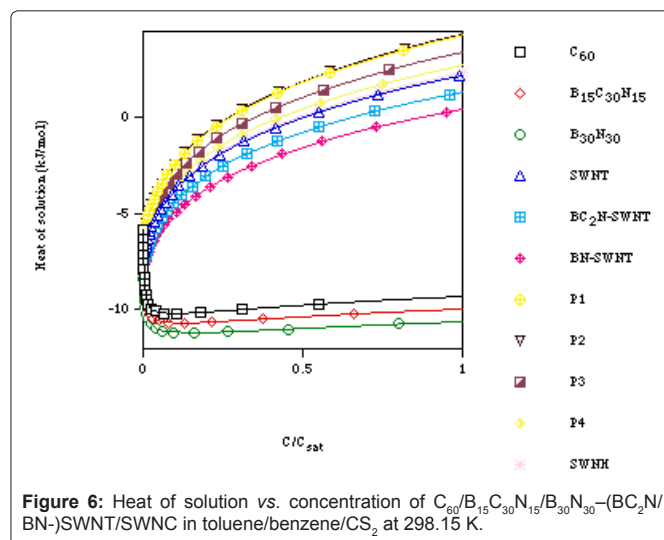

Figure 6: Heat of solution *vs.* concentration of C₆₀/$B_{15}C_{30}N_{15}$/$B_{30}N_{30}$–(BC₂N/BN-)SWNT/SWNC in toluene/benzene/CS₂ at 298.15 K.

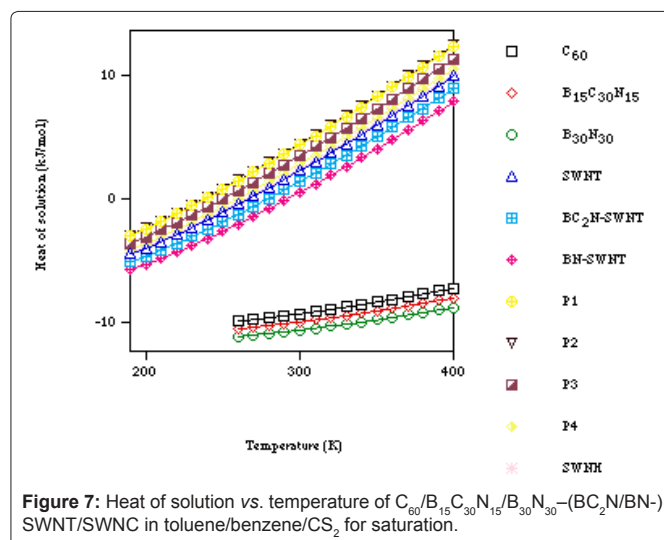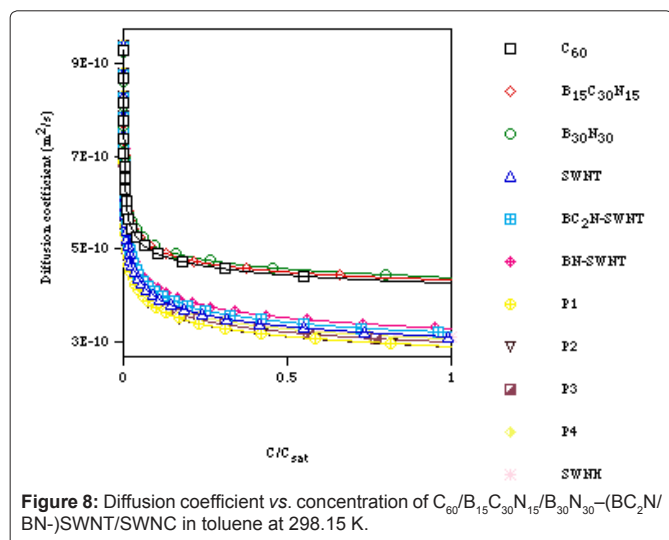**Figure 7:** Heat of solution *vs.* temperature of C₆₀/$B_{15}C_{30}N_{15}$/$B_{30}N_{30}$–(BC₂N/BN-)SWNT/SWNC in toluene/benzene/CS₂ for saturation.

68–70% for $B_{15}C_{30}N_{15}$, BC₂N-SWNT and BC₂N-SWNCs, as compared with that for $B_{15}C_{30}N_{15}$ molecule. For BC₂N-SWNT (bundlet), diffusion coefficient decays by 28%, and for BC₂N-SWNCs (bundlet) by 28–31%, with regard to $B_{15}C_{30}N_{15}$ (droplet). Cluster formation close to saturation decreases diffusion coefficients by 56%, 67% and 67–69% for $B_{30}N_{30}$, BN-SWNT and BN-SWNCs, as compared with that for $B_{30}N_{30}$ molecule. For BN-SWNT (bundlet), diffusion coefficient decays by 26%, and for BN-SWNCs (bundlet), by 26–29% with regard to $B_{30}N_{30}$ (droplet).

Conclusion

From the discussion of the present results, the following conclusions can be drawn.

1. The packing structures were deduced by fitting the voids between close-packed spheres. Several criteria reduced the analysis to a manageable quantity of properties: packing closeness, dimension, and efficiency. A model predicted packing properties. A non-computationally intensive approach, object clustering plus property prediction, allowed assessing calculation reliability, solving problem, and presenting applications.

Figure 5: Cluster distribution saturated in CS₂ at 298.15 K of C₆₀/$B_{15}C_{30}N_{15}$/$B_{30}N_{30}$–(BC₂N/BN-)SWNT/SWNH.

Figure 8: Diffusion coefficient *vs.* concentration of C$_{60}$/B$_{15}$C$_{30}$N$_{15}$/B$_{30}$N$_{30}$–(BC$_2$N/BN-)SWNT/SWNC in toluene at 298.15 K.

2. The packing efficiencies and interaction-energy parameters of nanocones are intermediate between those of C$_{60}$ and tubes: therefore, an in-between behaviour was expected for cones; however, cones result closer to tubes. The tube-like behaviour is observed in cones, whose properties are calculated closer to tubes. The packing efficiency and interaction-energy parameters of horns are closest to those of tubes: most tube-like behaviour is observed and properties are calculated closest to tubes. Large structural asymmetry in different types of cones, characterized by the number of pentagons (1–5), distinguished the calculated properties, especially for cones with two pentagons P2; e.g. the heat of solution varied: P2≈P1>P3>P4>SWNH≈SWNT >> C$_{60}$.

3. BC$_2$N and BN will be stable, especially species that are isoelectronic with C-analogues. Specific morphologies were observed for tube ends, which are suggested to result from B–N units. The chemical strain that 60° disclinations introduce in B$_{30}$N$_{30}$ governs its structural difference with C tubes.

4. Some systems are dominated by the isolated-pentagon-rule structures while some others, by the non-isolated-pentagon-rule ones.

Further work will explore similar nanostructure nature: possible generalization of conclusions to more complex systems: (1) there is way of bypassing weak homonuclear bonding in closed B$_x$N$_x$, involving replacement of 5-membered rings by 4-membered B$_2$N$_2$ annuli, ensuring perfect heteroatom alternation, and (2) BN/AlN tubes/heterojunctions.

Acknowledgments

References

1. Faraday M (1857) The Bakerian Lecture: Experimental relations of gold (and other metals) to light. Philos Trans R Soc London 147: 145-181.

2. Murphy CJ, Thompson LB, Alkilany AM, Sisco PN, Boulos SP, et al. (2010) The many faces of gold nanorods. J Phys Chem Lett 1: 2867-2875.

3. Balaban AT, Klein DJ, Liu X (1994) Graphitic cones. Carbon 32: 357-359.

4. Klein DJ (2002) Topo-combinatoric categorization of quasi-local graphitic defects. Phys Chem Chem Phys 4: 2099-2110.

5. Klein DJ, Balaban AT (2006) The eight classes of positive-curvature graphitic nanocones. J Chem Inf Model 46: 307-320.

6. Klein DJ (1992) Aromaticity *via* Kekule structures and conjugated circuits. J Chem Educ 69: 691-694.

7. Misra A, Klein DJ, Morikawa T (2009) Clar theory for molecular benzenoids. J Phys Chem A 113: 1151-1158.

8. Misra A, Schmalz TG, Klein DJ (2009) Clar theory for radical benzenoids. J Chem Inf Model 49: 2670-2676.

9. Balaban AT, Klein DJ (2009) Claromatic carbon nanostructures. J Phys Chem C 113: 19123-19133.

10. Klein DJ, Balaban AT (2011) Clarology for conjugated carbon nano-structures: Molecules, polymers, graphene, defected graphene, fractal benzenoids, fullerenes, nano-tubes, nano-cones, nano-tori, *etc*. Open Org Chem J 5: 27-61.

11. Tamura R, Tsukada M (1995) Electronic states of the cap structure in the carbon nanotube. Phys Rev B 52: 6015-6026.

12. Kim P, Odom TW, Huang JL, Lieber CM (1999) Electronic density of states of atomically resolved single-walled carbon nanotubes: Van Hove singularities and end states. Phys Rev Lett 82: 1225-1228.

13. Carroll DL, Redlich P, Ajayan PM, Charlier JC, Blase X, et al. (1997) Electronic structure and localized states at carbon nanotube tips. Phys Rev Lett 78: 2811-2814.

14. Jiang DL, Aida T (1997) Photoisomerization in dendrimers by harvesting of low-energy photons. Nature 388: 454-456.

15. Kroto HW (1987) The stability of the fullerenes C$_n$, with *n* = 24, 28, 32, 36, 50, 60 and 70. Nature 329: 529-531.

16. Han J, Jaffe R (1998) Energetics and geometries of carbon nanocone tips. J Chem Phys 108: 2817-2823.

17. Tagmatarchis N, Maigne A, Yudasaka M, Iijima S (2006) Functionalization of carbon nanohorns with azomethine ylides: Towards solubility enhancement and electron-transfer processes. Small 2: 490-494.

18. Pagona G, Sandanayaka ASD, Araki Y, Fan J, Tagmatarchis N, et al. (2007) Covalent functionalization of carbon nanohorns with porphyrins: Nanohybrid formation and photoinduced electron and energy transfer. Adv Funct Mater 17: 1705-1711.

19. Cioffi C, Campidelli S, Brunetti FG, Meneghetti M, Prato M (2006) Functionalisation of carbon nanohorns. Chem Commun 2129-2131.

20. Cioffi C, Campidelli S, Sooambar C, Marcaccio M, Marcolongo G, et al. (2007) Synthesis, characterization, and photoinduced electron transfer in functionalized single wall carbon nanohorns. J Am Chem Soc 129: 3938-3945.

21. Pagona G, Tagmatarchis N, Fan J, Yudasaka M, Iijima S (2006) Cone-end functionalization of carbon nanohorns. Chem Mater 18: 3918-3920.

22. Zhu J, Kase D, Shiba K, Kasuya D, Yudasaka M, et al. (2003) Binary nanomaterials based on nanocarbons: A case for probing carbon nanohorns' biorecognition properties. Nano Lett 3: 1033-1036.

23. Pagona G, Sandanayaka ASD, Araki Y, Fan J, Tagmatarchis N, et al. (2006) Electronic interplay on illuminated aqueous carbon nanohorn–porphyrin ensembles. J Phys Chem B 110: 20729-20732.

24. Pagona G, Fan J, Maigne A, Yudasaka M, Iijima S, Tagmatarchis N (2007) Aqueous carbon nanohorn–pyrene–porphyrin nanoensembles: Controlling charge-transfer interactions. Diam Relat Mater 16: 1150-1153.

25. Xia X, Jelski DA, Bowser JR, George TF (1992) MNDO study of boron-nitrogen analogues of buckminsterfullerene. J Am Chem Soc 114: 6493-6496.

26. Silaghi-Dumitrescu I, Haiduc I, Sowerby DB (1993) Fully inorganic (carbon-free) fullerenes? The boron-nitrogen case. Inorg Chem 32: 3755-3758.

27. Hamilton EJM, Dolan SE, Mann CM, Colijn HO, McDonald CA, et al. (1993) Preparation of amorphous boron nitride and its conversion to a turbostratic, tubular form. Science 260: 659-661.

28. Hamilton EJM, Dolan SE, Mann CM, Colijn HO, Shore SG (1995) Preparation

of amorphous boron nitride from the reaction of haloborazines with alkali metals and formation of a novel tubular morphology by thermal annealing. Chem Mater 7: 111-117.

29. Loiseau A, Willaime F, Demoncy N, Hug G, Pascard H (1996) Boron nitride nanotubes with reduced numbers of layers synthesized by arc discharge. Phys Rev Lett 76: 4737-4740.

30. Rubio A, Corkill JL, Cohen ML (1994) Theory of graphitic boron nitride nanotubes. Phys Rev B 49: 5081-5084.

31. Bourgeois L, Bando Y, Shinozaki S, Kurashima K, Sato T (1999) Boron nitride cones: Structure determination by transmission electron microscopy. Acta Cryst A 55:168-177.

32. Bourgeois L, Bando Y, Han WQ, Sato T (2000) Structure of boron nitride nanoscale cones: Ordered stacking of 240º and 300º disclinations. Phys Rev B 61: 7686-7691.

33. Terauchi M, Tanaka M, Suzuki K, Ogino A, Kimura K (2000) Production of zigzag-type BN nanotubes and BN cones by thermal annealing. Chem Phys Lett 324: 359-364.

34. Mota R, Machado M, Piquini P (2003) Structural and electronic properties of 240˚ nanocones. Physica Status Solidi (c) 0: 799-802.

35. Machado M, Piquini P, Mota R (2003) Energetics and electronic properties of BN nanocones with pentagonal rings at their apexes. Eur Phys J D 23: 91-93.

36. Machado M, Piquini P, Mota R (2003) Electronic properties of selected BN nanocones. Materials Characterizaton 50: 179-182.

37. Machado M, Mota R, Piquini P (2003) Electronic properties of BN nanocones under electric fields. Microelectron J 34: 545-547.

38. Machado M, Piquini P, Mota R (2004) Charge distributions in BN nanocones: Electric field and tip termination effects. Chem Phys Lett 392: 428-432.

39. Machado M, Piquini P, Mota R (2005) The influence of the tip structure and the electric field on BN nanocones. Nanotechnology 16: 302-306.

40. Thesing LA, Piquini P, Kar T (2006) Theoretical investigation on the stability and properties of a (10,0) BN–AlN nanotube junction. Nanotechnology 17: 1637-1641.

41. Miyamoto Y, Rubio A, Cohen ML, Louie SG (1994) Chiral tubules of hexagonal BC₂N. Phys Rev B 50: 4976-4979.

42. Tenne R, Margulis L, Genut M, Hodes G (1992) Polyhedral and cylindrical structures of tungsten disulphide. Nature 360: 444-446.

43. Margulis L, Salitra G, Tenne R, Talianker M (1993) Nested fullerene-like structures. Nature 365: 113-114.

44. Weng-Sieh Z, Cherrey K, Chopra NG, Blase X, Miyamoto Y, et al. (1995) Synthesis of BₓCᵧNᵤ nanotubules. Phys Rev B 51: 11229-11232.

45. Chopra NG, Luyken RJ, Cherrey K, Crespi VH, Cohen ML, et al. (1995) Boron nitride nanotubes. Science 269: 966-967.

46. Terrones M, Benito AM, Manteca-Diego C, Hsu WK, Osman OI, et al. (1996) Pyrolytically grown BₓCᵧNᵤ nanomaterials: Nanofibres and nanotubes. Chem Phys Lett 257: 576-582.

47. Kohler-Redlich P, Terrones M, Manteca-Diego C, Hsu WK, Terrones H, et al. (1999) Stable BC₂N nanostructures: Low-temperature production of segregated C/BN layered materials. Chem Phys Lett 310: 459-465.

48. Madden JDW (2009) Stiffer than steel. Science 323: 1571-1572.

49. Betke U, Henk M (2000) Densest lattice packings of 3-polytopes. Comput Geom 16: 157-186.

50. Chen ER, Engel M, Glotzer SC (2010) Dense crystalline dimer packings of regular tetrahedra. Discrete Comput Geom 44: 253-280.

51. Kallus Y, Elser V, Gravel S (2010) Dense periodic packings of tetrahedra with small repeating units. Discrete Comput Geom 44: 245-252.

52. Baker J, Kudrolli A (2010) Maximum and minimum stable random packings of Platonic solids. Phys Rev E 82: 061304–1-5.

53. Torrens F, Castellano G (2005) Cluster origin of the solubility of single-wall carbon nanotubes. Comput Lett 1: 331-336.

54. Torrens F, Castellano G (2007) Cluster nature of the solvation features of single-wall carbon nanotubes. Curr Res Nanotech 1: 1-29.

55. Torrens F, Castellano G (2007) Effect of packing on the cluster nature of C nanotubes: An information entropy analysis. Microelectron J 38: 1109-1122.

56. Torrens F, Castellano G (2007) Cluster origin of the transfer phenomena of single-wall carbon nanotubes. J Comput Theor Nanosci 4: 588-603.

57. Torrens F, Castellano G (2007) Asymptotic analysis of coagulation–fragmentation equations of carbon nanotube clusters. Nanoscale Res Lett 2: 337-349.

58. Torrens F, Castellano G (2011) (Co-)solvent selection for single-wall carbon nanotubes: *Best* solvents, acids, superacids and guest–host inclusion complexes. Nanoscale 3: 2494-2510.

59. Torrens F, Castellano G (2010) Cluster nature of the solvent features of single-wall carbon nanohorns. Int J Quantum Chem 110: 563-570.

60. Torrens F, Castellano G (2012) *Bundlet* model for single-wall carbon nanotubes, nanocones and nanohorns. Int J Chemoinf Chem Eng 2: 48-98.

61. Torrens F, Castellano G (2013) Solvent features of cluster single-wall C, BC₂N and BN nanotubes, cones and horns. Microelectron Eng.

62. Bezmel'nitsyn VN, Eletskii AV, Okun MV (1998) Fullerenes in solutions. Phys–Usp 41: 1091-1114.

63. Gasser U, Weeks ER, Schofield A, Pusey PN, Weitz DA (2001) Real-space imaging of nucleation and growth in colloidal crystallization. Science 292: 258-262.

64. Notman R, Noro M, O'Malley B, Anwar J (2006) Molecular basis for dimethylsulfoxide (DMSO) action on lipid membranes. J Am Chem Soc 128: 13982-13983.

65. Haluska CK, Riske KA, Marchi-Artzner V, Lehn JM, Lipowsky R, et al. (2006) Time scales of membrane fusion revealed by direct imaging of vesicle fusion with high temporal resolution. Proc Natl Acad Sci U S A 103: 15841-15846.

66. Neu JC, Cañizo JA, Bonilla LL (2002) Three eras of micellization. Phys Rev E Stat Nonlin Soft Matter Phys 66: 061406.

67. Betke U, Henk M (2000) Densest lattice packings of 3-polytopes. Comput Geom 16: 157-186.

68. Conway JH, Torquato S (2006) Packing, tiling, and covering with tetrahedra. Proc Natl Acad Sci U S A 103: 10612-10617.

69. Jiao Y, Torquato S (2011) Communication: A packing of truncated tetrahedra that nearly fills all of space and its melting properties. J Chem Phys 135: 151101.

Author Affiliations

¹Institut Universitari de Ciència Molecular, Universitat de València, Edifici d'Instituts de Paterna, P. O. Box 22085, E-46071 València, Spain
²Facultad de Veterinaria y Ciencias Experimentales, Universidad Católica de Valencia San Vicente Mártir, Guillem de Castro-94, E-46001 València, Spain